

AdvReal: Adversarial Patch Generation Framework with Application to Adversarial Safety Evaluation of Object Detection Systems

Yuanhao Huang^{a,b}, Yilong Ren^{a,c,*}, Jinlei Wang^{b,d}, Lujia Huo^{b,d}, Xuesong Bai^{a,b}, Jinchuan Zhang^a, Haiyang Yu^{a,c}

^a*School of Transportation Science and Engineering, Beihang University, Kejiyuan Rd, Haidian District, 100191, Beijing, P.R China*

^b*State Key Lab of Intelligent Transportation System, Kejiyuan Rd, Haidian District, 100191, Beijing, P.R China*

^c*Zhongguancun Laboratory, Haidian District, 100191, Beijing, P.R China*

^d*Aviation Academy, Inner Mongolia University of Technology, Aimin Street, Hohhot, 010051, Inner Mongolia, P.R China*

Abstract

Autonomous vehicles are typical complex intelligent systems with artificial intelligence at their core. However, perception methods based on deep learning are extremely vulnerable to adversarial samples, resulting in safety accidents. How to generate effective adversarial examples in the physical world and evaluate object detection systems is a huge challenge. In this study, we propose a unified joint adversarial training framework for both 2D and 3D samples to address the challenges of intra-class diversity and environmental variations in real-world scenarios. Building upon this framework, we introduce an adversarial sample reality enhancement approach that incorporates non-rigid surface modeling and a realistic 3D matching mechanism. We compare with 5 advanced adversarial patches and evaluate their attack performance on 8 object detectors, including single-stage, two-stage, and transformer-based models. Extensive experiment results in digital and physical environments demonstrate that the adversarial textures generated by our method can effectively mislead the target detection model. Moreover, proposed method demonstrates excellent robustness and transferability under multi-angle attacks, varying lighting conditions, and different distance in the physical world. The demo video and code can be obtained at <https://github.com/Huangyh98/AdvReal.git>.

Keywords: Adversarial patch, Object detection system, Reality enhanced, AI safety, Autonomous driving

1. Introduction

With the rapid advancement of artificial intelligence (AI), autonomous vehicles (AVs) have become widely adopted worldwide. Drivable area detection and object detection are the primary actors in any autonomous driving(AD) technology Zhang et al. (2022); Giri et al. (2025). Although the algorithms have achieved significant breakthroughs in performance, the frequent traffic accidents involving autonomous vehicles have raised public concerns about the safety and robustness of their perception systems. Consequently, the systematic testing and evaluation of object detection algorithms have become a prominent research focus.

Currently, AD object detection systems face two primary risks: natural scenario risks and adversarial scenario risks. Natural scenario risks stem from variations in the real environment, such as changes in lighting, weather, and the behavior of traffic participants Swerdlow et al. (2024). The performance of perceptive system are typically simulated and assessed through scenario generation techniques. In contrast, adversarial scenario risks involve malicious attackers employing adversarial

attacks to disrupt the normal operation of perception systems in both digital and physical domains Huang et al. (2024); Ran et al. (2025); Hu et al. (2023). Notably, physical attacks directly target objects in the real world, effectively bridging the digital and physical realms to produce a more potent effect. Such attacks can cause the autonomous driving system to fail in accurately detecting and localizing objection, which in turn may lead to hazardous driving decisions Fang et al. (2024); Bai et al. (2024).

The physical adversarial attack patch can be used to effectively evaluate the security of the target detection system Zhang et al. (2021). The adversarial patch for pedestrian detection was first introduced by AdvPatch Brown et al. (2017). By optimizing and generating adversarial patches, this approach effectively evades target detectors in the physical world, although it is limited to static objects. Subsequently, researchers have proposed a variety of patch-based physical adversarial attack methods, such as AdvTshirt Xu et al. (2020), AdvTexture Hu et al. (2022), and T-SEA Huang et al. (2023). In addition, techniques like NatPatch Hu et al. (2021) and AdvCaT Hu et al. (2023) have been developed for natural-looking and camouflaged attacks. Previous studies demonstrated strong adversarial attack performance in small-scale digital tests, yet they did not account for the multifaceted effects present in real-world environments.

Researchers found out that patch attacks' threaten may pose a smaller threat than previously believed, and that the success

*Corresponding author

Email addresses: yuanhao_huang@buaa.edu.cn (Yuanhao Huang), yilongren@buaa.edu.cn (Yilong Ren), 20231800822@imut.edu.cn (Jinlei Wang), 20231100544@imut.edu.cn (Lujia Huo), xs_bai@buaa.edu.cn (Xuesong Bai), 22376270@buaa.edu.cn (Jinchuan Zhang), hyyu@buaa.edu.cn (Haiyang Yu)

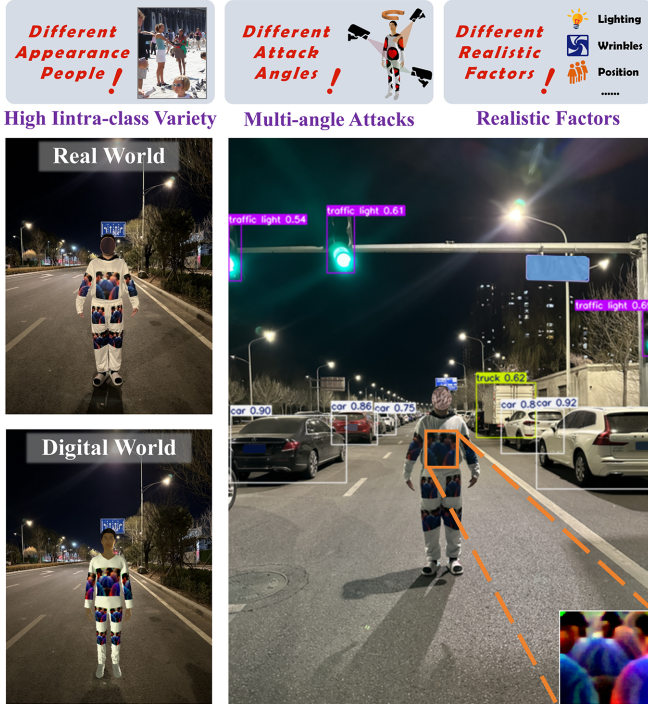


Figure 1: In response to multi-dimensional realistic challenges, performance of proposed adversarial patches in the physical world.

rate observed in simple digital simulations does not necessarily translate to real-world effectiveness Hingun et al. (2023). In pedestrian detection tasks, factors such as intra-class diversity, ambient lighting, and clothing wrinkles can all diminish the performance of adversarial patches Wang et al. (2024). For instance, applying patches to three-dimensional objects may lead to geometric distortions due to perspective projection effects Mahima et al. (2024). The discrepancy between simplified adversarial training in digital environments and the complex, dynamic nature of the physical world is the primary challenge in successfully applying adversarial patches Cui et al. (2024).

In this study, we proposed a reality-enhanced adversarial training framework called AdvReal. Through realistic enhancement and joint optimization of samples in both two-dimensional (2D) and three-dimensional (3D) spaces, more effective adversarial patch are generated for the physical world. The framework comprises three modules. The patch adversarial module refines patches in 2D and synthesizes samples that capture intra-class diversity. The realistic enhancement module processes 3D models to produce lifelike adversarial samples. And the joint optimization module concurrently refines both 2D and 3D adversarial samples to yield robust patches for complex physical world, shown in Fig. 1. The main contributions of this work are as follows:

- 1) Designed a general joint adversarial training framework for both 2D and 3D samples to overcome the challenges posed by intra-class diversity and variations in real-world environments during patch training.
- 2) Proposed an adversarial sample reality enhancement method based on non-rigid surface modeling and a real-

istic matching mechanism in 3D space. By simulating realistic factors, including cloth wrinkles and lighting conditions in the physical world, adversarial training and object detection evaluation can be effectively achieved using realistic 3D targets.

- 3) Numerous sets of experiments were conducted in both digital and physical environments, and we analyzed the underlying attack mechanism of the patch using visualization methods. Our quantitative and qualitative results show that the generated adversarial patch achieves a higher attack success rate, improved robustness, and superior transferability against pedestrian detectors compared to existing methods.

The remainder of this paper is organized as follows. Section 2 surveys related work on adversarial patches, the evasion of person detectors, and the practical challenges posed by adversarial attacks. Section 3 formalizes the research problem and presents the proposed methodology. Section 4 describes the simulation environment and experimental setup, and reports results obtained in both digital and physical settings. Section 5 discusses the advantages and limitations of the approach in light of the experimental findings. Finally, Section 6 concludes the study and outlines directions for future research.

2. Related works

2.1. Adversarial Patch

Compared to digital perturbations added directly to images Xiao et al. (2025), adversarial patches present a unique capability to attack detectors in the physical world. Since these patches are installed before the camera imaging process, they pose a greater threat to autonomous driving perception system and are of greater practical significance.

As a typical sparse perturbation, the adversarial patch efficiently creates patches that can universally degrade the accuracy of the classification Williams and Li (2024). In the context of traffic sign detection, Zhou et al. investigated how adversarial patches can manipulate AVs by making traffic signs unrecognizable or misclassified, showcasing the real-world implications of such attacks Zhou et al. (2024). Adversarial patches are also widely used in face recognition, where wearable masks Liu et al. (2024) or even tiny stickers Wei et al. (2022) can be generated to mislead deep neural networks. Therefore, adversarial patches have been widely used to evaluate the security and reliability of object detection system.

2.2. Evade Person Detectors with Adversarial Patch

Humans are among the most critical traffic participants. Using adversarial patches to attack pedestrian detection system provides an effective means to evaluate their susceptibility to adversarial risks. Unlike objects such as traffic signs, which exhibit minimal intra-class variability, humans present significant intra-class diversity, making the detection task more challenging Abed et al. (2024).

A common approach involves optimizing adversarial patches by placing them on the body and minimizing the maximum bounding-box probability associated with human detection. AdvPatch was the first adversarial patch attack method to deceive pedestrian detectors by optimizing detection loss Thys et al. (2019). Similarly, TOG employs attack-specific gradients based on adversarial targets to cause detectors to either miss or misclassify pedestrians Chow et al. (2020). However, TOG does not account for applications in the physical world. Furthermore, a GAN-based generative strategy restricts the appearance of generated patches to ensure that they look natural and inconspicuous Guesmi et al. (2024). NatPatch achieves this by sampling optimal images from GANs Hu et al. (2021), resulting in adversarial patches that are both visually natural and highly effective in attacks. All of these methods rely on real images of diverse individuals, overlaying adversarial patches within bounding boxes in a digital environment in 2D picture.

2.3. Multiple realistic challenges

When adversarial patches are applied in the physical world, their attack effectiveness is significantly diminished or rendered entirely ineffective. This limitation arises because most prior studies have overlooked three critical real-world factors.

2.3.1. High level of intra-class variety

Pedestrians exhibit a high degree of intra-class variability, characterized by significant differences in appearance, posture, and dynamic motion. To address these variations, the SOTA pedestrian detection models leverage extensive training data sets and advanced feature extraction techniques to improve the robustness of the algorithms Ren et al. (2016a); Redmon (2018); Carion et al. (2020). Consequently, devising effective and generalized adversarial attack strategies requires exceptional adaptability and robustness. Simen Thys et al. were among the first to explore such attacks on targets with high intra-class variability, utilizing real images of diverse individuals Thys et al. (2019). Building on this, Zhou et al. proposed the PosePatch framework, a patch adaptation network for adversarial patch synthesis guided by perspective transformations and estimated human poses Zhou et al. (2025). These advancements underscore the importance of leveraging abundant intra-class training samples to significantly enhance the robustness and effectiveness of adversarial patches.

2.3.2. Multi-angle attacks

Traditional superposition training ensures that pedestrian detectors perform effectively when facing the patch but lacks robustness to varied angles or occlusions. To address the challenges posed by multi-angle perception attacks, AdvTexture introduces a scalable adversarial texture generation method based on ring cropping Hu et al. (2022). This approach can be applied to clothing of arbitrary shapes, allowing individuals wearing these garments to evade detection by human detectors from various angles. Furthermore, Arman Maesumi et al. proposed a framework for adversarial training using 3D modeling, which optimizes 3D adversarial cloaks through variations in poses,

spatial positions, and camera angles Maesumi et al. (2021). By conducting multi-angle adversarial training, the effectiveness of patches in multi-detection angle scenarios can be significantly improved Li et al. (2025); Hu et al. (2023).

2.3.3. Realistic factors

Accurately capturing all real-world variations through digital images of simulated patches for adversarial training and evaluation remains challenging Hingun et al. (2023). Modeling non-rigid object surfaces, such as clothing, during training and utilizing them for adversarial optimization poses a considerable challenge. For instance, Adv-Tshirt employs video frames of a person wearing a T-shirt with a checkerboard pattern as training data, mapping the patch onto a distorted checkerboard for training Xu et al. (2020). AdvCaT proposes a non-rigid deformation method based on TopoProj to simulate wrinkles on human clothing Hu et al. (2023). The inclusion of adversarial training methods that account for non-rigid wrinkles enhances the robustness of patches in real-world physical environments. In addition, Traditional patch superposition methods assume that patches are square and axis aligned and can be placed anywhere within the image. However, random rotation, cropping, and noise do not fully simulate real-world variations in lighting, noise, and posture. REAP proposes an improved method that incorporates geometric and lighting transformations to enable large-scale performance evaluation of patches, particularly traffic signal signs Hingun et al. (2023). In summary, the reality augmentation method can effectively improve the robustness of the adversarial patch for realistic challenges.

3. Methodology

In this section, we first formulate the object and define the optimization problem. Then, we demonstrate the details of the proposed method, including adversarial generation framework, realistic matching module, and joint optimization strategy.

3.1. Problem Definition

In this study, we conduct a joint attack on 2D high-level intra-class variety data and 3D augmented reality data. The ultimate goal is to effectively reduce the accuracy of adversarial patches successfully recognized by human detectors in the real world. Specifically, let $P(X, Y)$ represent the joint distribution of pedestrian data, where $X \subseteq \mathbb{R}^d$ is the input image space and $Y \subseteq \{1, \dots, C\}$ is the label space. A pretrained pedestrian detector $f_h : [-1, 1]^d \rightarrow [0, 1]^C$ maps the input $x \in X$ to a probability distribution over C classes, with the predicted label $\hat{y} = \arg \max_c f_c(x)$. Given samples $\{(x_1, y_1), \dots, (x_n, y_n)\} \sim P(X, Y)$, the goal of adversarial attacks is to construct a perturbed input $x^{adv} = x + \delta$, where $\|\delta\|_p \leq \epsilon$, such that the detector $f(x^{adv})$ misclassifies x^{adv} into a label $\hat{y} \neq y$.

The optimization problem is then formulated as Eq. 1:

$$\delta^* = \arg \min_{\delta} \frac{1}{n} \sum_{i=1}^n \mathcal{L}(f_h(x_i + \delta), y_i) + \lambda \mathcal{R}(\delta), \quad (1)$$

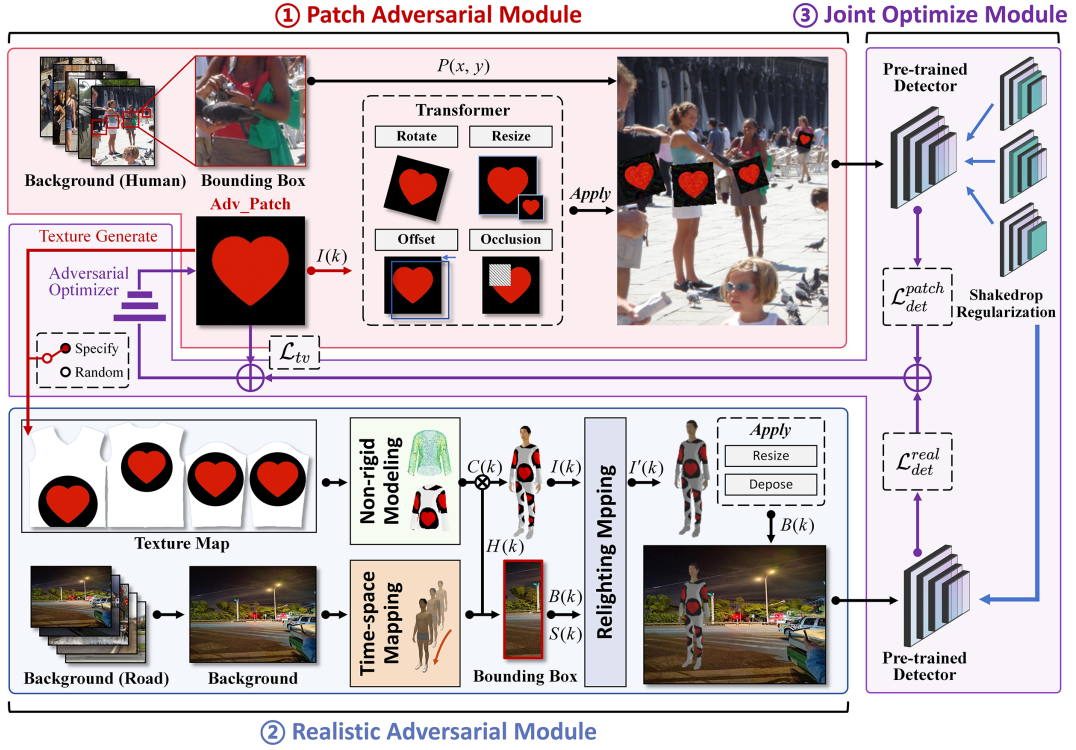


Figure 2: Overview of the proposed adversarial attack method.

where $\mathcal{L}(f(x_i + \delta), y_i)$ measures the discrepancy between the detector's prediction on the perturbed input $x_i + \delta$ and the true label y_i . The regularization term $\mathcal{R}(\delta)$ ensuring the smoothness of the adversarial patch, thereby reducing visual artifacts, and improving the generalization and transferability of the patch by preventing over-fitting. The coefficient λ balances the adversarial loss and the regularization term, ensuring that the adversarial patch is both effective in disrupting the detector's performance and robust enough to generalize across diverse real-world scenarios and detection architectures.

3.2. Adversarial Generation Framework

To address the limitations of existing methods, this paper introduces a novel framework for generating adversarial patches designed to deceive human detectors in real-world scenarios. The proposed framework, named AdvReal, jointly optimizes 2D and 3D adversarial losses, effectively tackling challenges such as high intra-class variability, multi-angle attack scenarios, and complex real-world factors. Unlike traditional adversarial patches applied to traffic signs or rigid materials, our method focuses on patches on non-rigid clothing, ensuring effectiveness from multiple angles in realistic scenarios.

As illustrated in Fig.2, the AdvReal framework consists of three key modules: the Patch Adversarial Module, the Realistic Enhancement Module, and the Joint Optimization Module. These modules work collaboratively to enhance the adversarial performance and realism of the generated patches.

3.2.1. Patch Adversarial Module

To enhance the generalization performance of intra-class adversarial attacks against human detectors, the Patch Adversarial

Module leverages a diverse human dataset for 2D adversarial training. In this module, patches are placed at the center of the human bounding boxes within the dataset, followed by transformation operations such as rotation, resizing, offsetting, and occlusion. These transformations ensure the robustness of the adversarial patches under varying conditions. The synthesized images, comprising patches overlaid on humans and their backgrounds, are then utilized for 2D adversarial training to improve attack efficacy.

3.2.2. Realistic Enhance Module

This module employs 3D meshes to model humans, clothing, and pants, attaching the texture map generated by the adversarial patch to the clothing. With the **time-space enhance strategy** refer to Sec.3.3, 3D adversarial clothes with reasonable folds are rendered. The realistic matching mechanism refer to Sec.3.4 processes the rendered human images by first aligning them to realistic distance, size, elevation, and azimuth to ensure accurate spatial representation. And then applying nonlinear adjustments to brightness and contrast to enhance the lighting conditions for improved realism, seamlessly integrating both geometric and lighting aspects to produce highly realistic human images. Finally, the resized human images are synthesized onto decomposed background images for 3D adversarial training. Notably, the Patch Adversarial Module and the Realistic Enhance Module operate synchronously during each batch training process.

3.2.3. Joint Optimization Module

The synthetic images produced by the Patch Adversarial Module and the Realistic Enhance Module are fed into the pre-

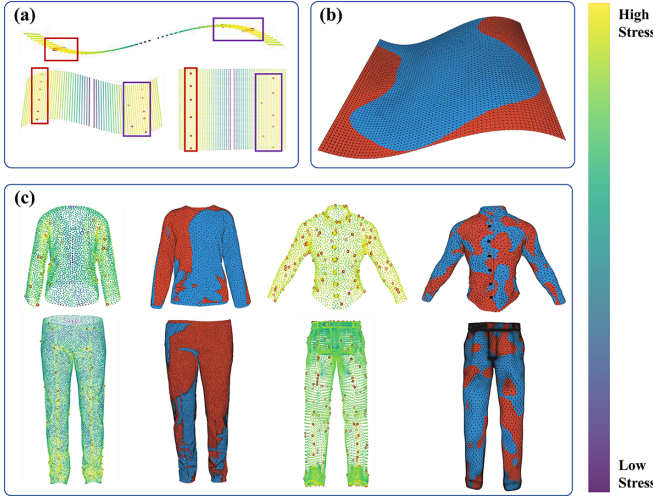


Figure 3: Schematic diagram and results display of non-rigid surfaces modeling. (a) Mesh of the simulated cloth, with control points strategically distributed in high-stress regions. (b) Deformation result after applying random target points with smoothing, exhibiting no abnormal distortions. (c) Non-rigid modeling and deformation outcomes for both shirt and pants.

trained human detector targeted for attack. During this process, the detector randomly freezes certain layers, and the output is used to compute the adversarial loss. The appearance of the adversarial patch is iteratively optimized by minimizing a combined loss function, which includes 2D detection loss, 3D detection loss, and Total Variation (TV) loss. The **joint optimization mechanism** refer to Sec.3.5 ensures that the disguised patch achieves high effectiveness across both 2D and 3D detection scenarios.

3.3. Non-rigid surfaces modeling

Methods based on shear transformation or 3D thin plate spline(3D-TPS) disregarding the nonlinear deformation characteristics of real fabrics Wei et al. (2024). Such an simplification gives rise to two crucial shortcomings in adversarial pattern deployment: (1) geometric discontinuities in high-curvature regions of cloth folds; and (2) physically implausible stretching artifacts during dynamic body movements, leading to noticeable texture distortions.

To improve realism in fabric deformation, we integrate a physics-driven approach that analyzes the motion flow of the clothes mesh to estimate load-bearing stress points. These stress points serve as key locations for generating natural, non-rigid folds, ensuring diverse but realistic fabric behavior even under consistent adversarial training motions Gundogdu et al. (2020).

We estimate the stress tensor at each vertex \mathbf{v}_i in the garment mesh $\mathcal{M} = (\mathcal{V}, \mathcal{E})$, where stress is accumulated from neighboring vertices:

$$\sigma_i = \sum_{j \in N(i)} w_{ij} \|\mathbf{v}_j - \mathbf{v}_i\|_2 \quad (2)$$

where w_{ij} is the adjacency weight, and $N(i)$ denotes the neighboring vertices of \mathbf{v}_i . As shown in Fig. 3, High-stress areas correspond to fabric regions experiencing significant force transmission, typically near joints and constrained areas. Regions

with significant force transmission—typically near joints and constrained areas—are identified by selecting vertices that satisfy:

$$\mathcal{S} = \{p_i \mid \sigma_i > \sigma_{\text{thres}}\}, \quad (3)$$

where

$$\sigma(p_1) \geq \sigma(p_2) \geq \dots \geq \sigma(p_M), \quad (4)$$

Here, σ_{thres} is a predefined threshold to reduce computational complexity. After identifying the high-stress points \mathcal{S} . The final control point set C is then determined by enforcing a spatial isolation criterion:

$$C = \left\{ p_i \in \mathcal{S} \mid \forall p_j \in C, \|p_i - p_j\| \geq \frac{\gamma}{\sigma(p_i)} \right\}, \quad (5)$$

where

$$|C| = \max \{N_{\min}, \lfloor \rho |\mathcal{S}| \rfloor\}. \quad (6)$$

Here, γ is a minimum distance factor that ensures sufficient spatial separation between control points, ρ is a density ratio that determines the target number of control points, and N_{\min} is a predetermined lower bound on the number of control points.

To generate realistic fabric wrinkles while retaining design flexibility, we inject a stochastic perturbation term into the deformation function to capture the natural variability observed under similar body movements:

$$f(\mathbf{v}) = \mathbf{v} + \sum_{k=1}^K \mathbf{w}_k \phi(\|\mathbf{v} - \mathbf{c}_k\|) + \delta \mathbf{r}_i \quad (7)$$

where $\mathbf{r}_i \sim \mathcal{N}(0, \Sigma)$ is a Gaussian noise vector, and δ scales the perturbation. This ensures natural variations in generated wrinkles under similar body movements, enhancing the realism of adversarial textures.

However, unconstrained noise can produce physically implausible distortions. We regulate vertex displacements by imposing stress-dependent constraints:

$$\Delta \mathbf{v}_i = \min \left(1, \frac{\delta_{\max} \cdot (1 + \lambda \sigma_i)}{\|\Delta \mathbf{v}_i\|_2} \right) \cdot (\mathbf{v}'_i - \mathbf{v}_i) \quad (8)$$

where λ modulates the stress-dependent displacement expansion. This ensures regions with higher stress experience larger but controlled deformations, maintaining smoothness and physical consistency.

3.4. Realistic Matching Mechanism

In realistic scenarios, factors such as distance and illumination introduce challenges related to variations in scale, perspective, and lighting conditions. To enhance the realistic relevance of adversarial patch training and evaluation, we propose two complementary strategies: **time-space mapping** and **relight mapping**. First, time-space mapping is employed to generate pedestrian bounding boxes that accurately reflect real-world scales. Second, we introduce an optimization-based relight mapping approach to further enhance the visualization of the pedestrian detection model under diverse lighting conditions.

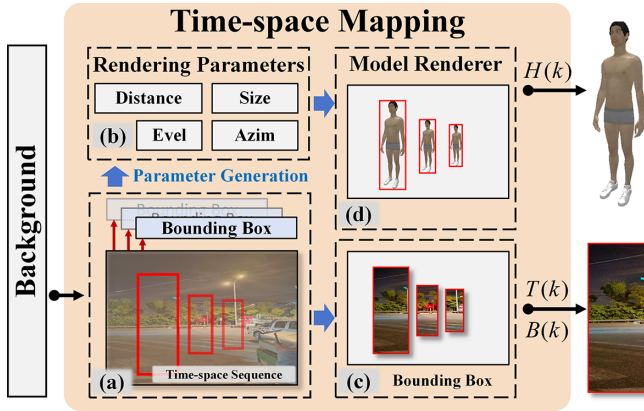


Figure 4: Flowchart of spatiotemporal mapping. (a) Select consecutive candidate bounding boxes that satisfy the perspective relationship in the background image. (b) Generate rendering parameters based on the positions of the selected bounding boxes. (c) Extract background image corresponding to the bounding box. (d) Generate rendering parameters for the person within the corresponding bounding box.

3.4.1. Time-space Mapping

We aim to render a human model that is more consistent with the time-space distribution to facilitate integration with the background. The method first randomly select a bounding box b_{human} with human proportions. The orientation of the human model is facing, represented by a direction vector $\mathbf{v}_{\text{orient}}$, is then determined. Based on this orientation, the bounding box is adjusted and scaled to generate two additional bounding boxes, b_{near} and b_{far} , which follow a perspective-based scaling rule. Specifically, as shown in Fig. 4 (a), we generate a near and a far rendering image at different positions of the same background according to the position of the first bounding box and the orientation of the character model. And the near bounding box b_{near} is larger, and the far bounding box b_{far} is smaller, with their sizes inversely proportional to the distance from the camera.

As shown in Fig. 4 (b), the rendering parameters including scale s , distance d , and orientation angles θ_e and θ_a from the geometric properties of the boxes can be derived. The azimuth angle θ_a is obtained by solving the inverse angle based on the facing direction of the human model.

These derived parameters guide the rendering process, where a differentiable renderer projects the adversarial texture onto a 3D human mesh, adjusting its distance, size, and azimuth. Crucially, the rendered model's silhouette (Fig. 4 (d)) is constrained to fit within the bounding box b_i 's coordinates (Fig. 4 (c)), ensuring geometric consistency when composited into the background. Subsequently, the human model $H(k)$ is used for combined rendering with the clothing $C(k)$ after non-rigid surface modeling. And the bounding box $B(k)$ and the background image slice $T(k)$ are used as input in Relighting mapping.

3.4.2. Relighting Mapping

In order to generate images for adversarial training, the rendered characters need to be fused with the background. The combination process can be expressed as Eq. 9:

$$\tilde{x}_{i+1}^{\text{adv}} = M \odot \tilde{R}_{i+1}^{\text{hum}} + (1 - M) \odot X, \quad (9)$$

Algorithm 1: Relighting-mapping optimisation

```

Input: real image  $I_r$ , rendered image  $I_0$ 
Output:  $(\alpha^*, \beta^*, \theta^*)$ 
1 Initialisation:
2  $\alpha_0, \beta_0, \theta_0$ ; // contrast, brightness, bias
   coeffs
3  $\lambda_\alpha, \lambda_\beta, \lambda_\theta$ ; // regularisation
4  $\eta, T$ ; // learning rate and iterations
5 for  $t \leftarrow 1$  to  $T$  do
6    $I'_0 \leftarrow \alpha I_0 + \beta + B_\theta(I_0, I_0)$ ;
7    $\mathcal{L}_{\text{sim}} \leftarrow 1 - \text{SSIM}(I'_0, I_r)$ ;
8    $\mathcal{L}_{\text{reg}} \leftarrow \lambda_\alpha(\alpha - 1)^2 + \lambda_\beta\beta^2 + \lambda_\theta\|\theta\|_2^2$ ;
9    $\mathcal{L}_{\text{tot}} \leftarrow \mathcal{L}_{\text{sim}} + \mathcal{L}_{\text{reg}}$ ;
10   $\varepsilon \leftarrow \varepsilon - \eta \nabla_\varepsilon \mathcal{L}_{\text{tot}}$ ,  $\varepsilon = [\alpha, \beta, \theta]$ ;
11  if  $\alpha \notin [\alpha_l, \alpha_h] \vee \beta \notin [\beta_l, \beta_h]$  then
12     $\alpha \leftarrow \text{clip}(\alpha, \alpha_l, \alpha_h)$ ;
13     $\beta \leftarrow \text{clip}(\beta, \beta_l, \beta_h)$ ;
14  else
15    continue;
16 return  $(\alpha^*, \beta^*, \theta^*)$ 

```

where $M \in \{0, 1\}^{H \times W}$ is a binary mask derived from the 3D human model, with $M = 1$ corresponding to the human texture and $M = 0$ to the background. $M \odot \tilde{R}_{i+1}^{\text{hum}}$ overlays the rendered human texture, including the adversarial patch, onto the human region, while $(1 - M) \odot X$ preserves the background texture.

In this study, we proposed an optimization method to adjust the contrast and brightness of the 3D rendered character to maximize its similarity with the background image while preserving its original texture. As shown in Alg. 1, we adjust the original image I_0 for contrast and brightness, obtaining the image I'_0 with altered lighting characteristics, and match it with the given real image I_r . The adjustment process is formulated as follows:

$$I'_0 = \alpha^* a \cdot I_0 + \beta^* + \theta^* \quad (10)$$

where, α is the contrast adjustment factor, β is the brightness adjustment factor, and θ is the bias coefficient. The bias coefficient is used to prevent excessive differences between the rendered image and the original texture. Our objective is to optimize the parameters α , β , and θ to minimize the total loss function, which consists of two main components: similarity loss and regularization loss.

To ensure that the rendered character matches the real background image, we use the Structural Similarity Index (SSIM) to quantify the similarity between the rendered image and the real image. Specifically, we first compute the similarity loss defined as $1 - f_s(I_0, I_r)$, ensuring that the rendered image I'_0 is structurally similar to the real image I_r . We then calculate the regularization terms to control the magnitude of the parameters α , β , and θ . These regularization terms prevent overfitting by penalizing large parameter values. The regularization terms apply penalties to overly large parameter values, ensuring model stability. Ultimately, the total loss function is the sum of the similarity loss \mathcal{L}_{sim} and the regularization loss \mathcal{L}_{reg} .

$$\mathcal{L}_{tot.} = \mathcal{L}_{sim} + \mathcal{L}_{reg}, \quad (11)$$

where

$$\begin{cases} \mathcal{L}_{sim} = 1 - f_s(I_o, I_r), \\ \mathcal{L}_{reg} = \lambda_\alpha(\alpha - 1)^2 + \lambda_\beta\beta^2 + \lambda_\theta\|\theta\|_2^2. \end{cases} \quad (12)$$

We use the Adam optimizer to optimize the parameters α , β , and the bias coefficient θ to minimize the total loss function. The proposed optimization method adjusts brightness and contrast of rendered image I'_o via linear transformations while employing a nonlinear correction to preserve texture features, to match the real image I_r .

3.5. Joint optimization mechanism

In this part, we introduce the joint loss framework proposed in this paper to address the challenges of high level of intra-class variety and realistic factors.

3.5.1. Detection Loss

The detection loss L_{det} operates by prioritizing bounding box predictions that achieve both high localization accuracy and confident classification, shown in eq. 13.

$$\mathcal{L}_{det}(p) = \max(s_{i,j} \mid IoU(b_{i,j}, b_{gt,j}) \geq \tau, l_{i,j} = 1) \quad (13)$$

Here, L_{det} evaluates predictions based on spatial alignment and semantic relevance. For each candidate box $b_{i,j}$, the loss ensures geometric consistency by verifying if its IoU with the ground truth $b_{gt,j}$ exceeds a threshold τ . Simultaneously, the binary indicator $l_{i,j}$ confirms its validity as a positive sample. The loss then selects the highest confidence score $s_{i,j}$ from all qualified candidates as the value of detection loss. In this study, both 2D detection loss L_{det}^{patch} and 3D detection loss L_{det}^{real} are calculated using this method.

3.5.2. Total variation loss (TV loss)

The total variation loss encourages spatial smoothness in the adversarial patch by penalizing abrupt pixel intensity changes. It is defined as:

$$\mathcal{L}_{tv}(p) = \sum_{i,j} (|p_{i+1,j} - p_{i,j}| + |p_{i,j+1} - p_{i,j}|), \quad (14)$$

where $p_{i,j}$ represents the pixel intensity at position (i, j) . The first term enforces smoothness along the horizontal direction, while the second term does so along the vertical direction. By minimizing TV loss, the optimization discourages high-frequency noise and unnatural artifacts, ensuring that the adversarial patch remains visually consistent and less perceptible.

3.5.3. Patch Optimize

During adversarial sample training, the detection model is treated solely as a fixed closed-box for loss calculation and gradient propagation during patch optimization. Inspired by stochastic depth Huang et al. (2016, 2023), we employ the *shakedrop regularization* mechanism that randomly adjusts

both the forward-output and backward-gradient flows in the residual block Yamada et al. (2018). Specifically, in the forward pass, we combine the identity mapping with the stacked layers' output to generate new feature representations. For an input feature x_{in} and the stacked layers' output $H(x_{in})$, the fusion rule is formulated as:

$$x_{out} = x_{in} + (\gamma_1 + \omega - \gamma_1 \cdot \omega) H(x_{in}),$$

where γ_1 is a Bernoulli random variable with $P(\gamma_1 = 1) = p_s$, and ω is sampled from a continuous uniform distribution $\omega \sim U(1 - k, 1 + k)$. Here, k is a predefined constant.

During backpropagation, let \mathcal{L} denote the loss function. The gradient adjustment follows the chain rule:

$$\mathcal{G}_{x_{in}} = \mathcal{G}_{x_{out}} \cdot \left(1 + (\gamma_2 + \omega - \gamma_2 \cdot \omega) \frac{\partial H}{\partial x_{in}} \right),$$

where γ_2 is another Bernoulli variable drawn from the same distribution as γ_1 . Through stochastic coefficient fusion in both forward propagation and gradient computation, this approach injects perturbations that enhance the generalization capability of adversarial samples.

The random perturbations effectively create multiple virtual model variants without requiring additional model training. Although the perturbation process does not directly update model parameters, it diversifies the computational pathways, enabling attackers to produce highly transferable adversarial samples using only a single glass-box model.

Building on these benefits, the adversarial patch is iteratively refined. At each step i , the next-step rendering of the human texture is defined as:

$$R^{\text{hum}}(p_{i+1}) = g(p_i + \epsilon \cdot \text{sign}(\nabla_p \mathcal{L}(f_h(x^{\text{adv}}(p)), y))), \quad (15)$$

where $f_h : [-1, 1]^d \rightarrow \mathbb{R}^C$ is a pre-trained human detection model mapping the adversarial image x^{adv} to class probabilities. The function $g(\cdot)$ renders the adversarial patch onto the 3D human model, ensuring its adaptation to the surface geometry.

The adversarial patch p_i is optimized to reduce the detection model's performance by applying a gradient-based update. $\epsilon \cdot \text{sign}(\nabla_p \mathcal{L}(f(x^{\text{adv}}(p)), y))$ adjusts the patch in the direction that maximally alters the model's prediction, where $\nabla_p \mathcal{L}$ is the gradient of the loss function with respect to the patch, $\epsilon > 0$ is the step size, and $\text{sign}(\cdot)$ extracts the gradient's sign.

4. Experiments

In this section, we conduct extensive experiments to verify the effectiveness of the proposed AdvReal method. We first describe the experimental setup and then compare it with SOTA methods in both the digital and physical world.

4.1. Experiments Setup

4.1.1. Dataset

In the **Patch Adversarial Module (2D adversarial)**, we employ the INRIA Person dataset Dalal and Triggs (2005) to train

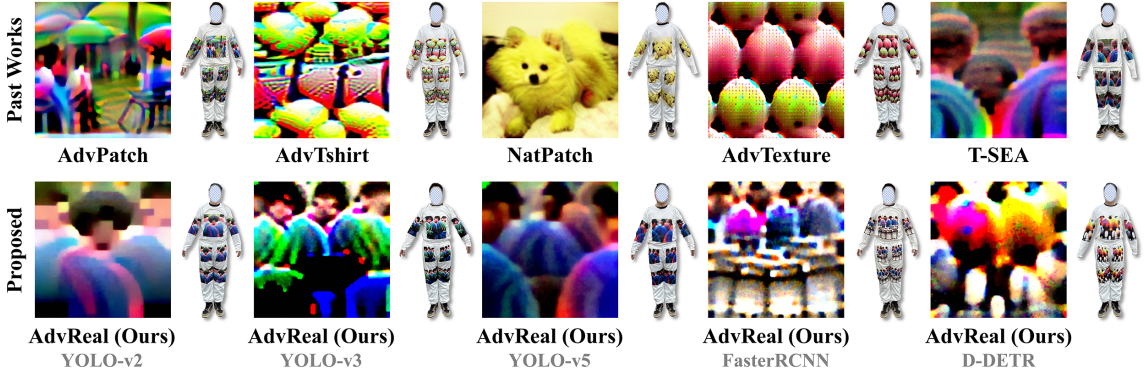


Figure 5: Adversarial patches of other advanced algorithms and ours.

and test our adversarial patch, which comprises 462 training images and 100 test images.

In the **Realistic Adversarial Module (3D adversarial)**, we randomly selected 562 traffic scene images from the nuScenes dataset Caesar et al. (2020), captured from six camera perspectives (Front, Front Right, Front Left, Back Right, Back Left, and Back), to serve as backgrounds for 3D rendering in evaluating our adversarial patches. Among these, 450 images were captured under adequate lighting and 112 under poor lighting. The daytime and nighttime images were randomly divided into a training set of 462 images and a test set of 100 images.

4.1.2. Victim Detector

We perform adversarial training and attacks on current mainstream object detectors, including single-stage, two-stage, and transformer-based architectures (shown in Tab. 1). The models are pre-trained on MS COCO dataset Lin et al. (2014). In particular, we conduct closed-box attack tests on SOTA detectors (YOLO-v8, v11, v12) in the physical world for the first time. Floating Point Operations (FLOPs) quantify the computational workload required by a model during inference and serve as an indicator of the model’s complexity. In general, models with higher complexity tend to exhibit improved robustness and generalization capabilities.

Table 1: Victim Detector for evaluating the effectiveness of adversarial patches, including single-stage, two-stage, and transformer-based models.

Detector	Features	FLOPs	Years	Cites
YOLO-v2		5.58	2017	Redmon and Farhadi (2017)
YOLO-v3	Single-stage	193.89	2018	Redmon and Farhadi (2018)
YOLO-v5		7.70	2020	Jocher et al. (2020)
YOLO-v8		8.7	2023	Jocher et al. (2023)
YOLO-v11	Single-stage (SOTA)	6.50	2024	Jocher and Qiu (2024)
YOLO-v12		6.50	2025	Tian et al. (2025)
Faster-RCNN	Two-stage	180.00	2016	Ren et al. (2016b)
D-DETR	Transformer-based	78.00	2021	Zhu et al. (2020)

4.1.3. Evaluation Metric

In the evaluation framework, we define that if the IoU between the detection box and the true box is less than 0.5, or the confidence is lower than 0.5, the attack is considered successful. We use multiple quantitative metrics to comprehensively evaluate the effectiveness of algorithm-generated adversarial patches, as follows:

- **Attacking Success Rate (ASR):** The percentage of adversarial samples that cause the detector to fail.
- **Precision:** The ratio of correct detections to total detections. Lower precision indicates that the detector is more effectively misled by the adversarial patch.
- **Recall:** The ratio of correctly detected ground-truth targets to all ground-truth targets. Lower recall signifies that more targets are missed due to the attack.
- **F1-Score:** The harmonic mean of precision and recall. A lower F1-score reflects an overall degradation in detection performance.
- **Average Confidence (AC):** The mean confidence score of the detector’s predictions. A lower AC indicates that the detector’s certainty in its detections is reduced due to the adversarial attack, reflecting weakened reliability in its outputs.

4.1.4. Experimental Details

During the digital train and evaluation, the distance from 3D human model to camera is limited in 1 to 4 meters. All rendered human models are at random angles and positions, and follow the principle of time-space mapping in Sec. 4.

In non-rigid surfaces modeling module, σ, γ, ρ in eq. 3 is set as 0.8, and γ, ρ in eq. 5 are set as 0.01, 0.2 respectively. The total number of training rounds is set to 800. The initial training patch size is set as 300×300 , the input image is 416×416 . We choose Adam as the optimizer and the learning rate is set as 0.01. All experiments are conducted with 16G NVIDIA GeForce RTX 4080 GPU.

4.1.5. Baseline

We compared our method *AdvReal* with both classic and state-of-the-art (SOTA) adversarial methods. The classic methods include *AdvPatch*Brown et al. (2017), *AdvTshirt*Xu et al. (2020), and *NatPatch*Hu et al. (2021), while the SOTA methods comprise *AdvTexture*Hu et al. (2022), *AdvCatH*u et al. (2023), and *T-SEA*Huang et al. (2023). In addition, we assess *White*, *Gray*, and *Random Noise* patches as control groups. For fairness, the areas of all adversarial patches on both rendered and

Table 2: Comparisons with existing detection attack methods. Compared with existing methods, the proposed AdvReal achieves the best performance on both glass-box attack and closed-box attack.

Method	ASR \uparrow (Glass-box)	ASR \uparrow (Closed-box)							ASR \uparrow (Closed-box Avg)
		YOLOv2	YOLOv3	YOLOv5	YOLOv8	YOLOv11	YOLOv12	F-RCNN	
White	1.08%	0.43%	2.60%	1.95%	5.63%	2.60%	0.22%	3.68%	2.44%
Gray	0.39%	0.43%	4.11%	4.98%	6.49%	3.90%	0.22%	6.71%	3.83%
Noise	0.22%	0.87%	5.19%	10.39%	4.55%	4.98%	0.43%	3.68%	4.30%
AdvPatch	33.55%	3.46%	51.52%	42.64%	22.51%	16.45%	6.06%	30.30%	24.71%
AdvTshirt	24.68%	12.77%	43.72%	35.28%	27.92%	15.80%	1.52%	31.39%	24.06%
NatPatch	6.06%	4.98%	16.23%	10.39%	8.87%	4.11%	0.22%	13.20%	8.29%
AdvTexture	55.63%	75.11%	69.05%	28.35%	22.29%	19.70%	13.64%	52.60%	40.11%
AdvCaT	0.00%	0.00%	0.00%	0.65%	0.43%	0.87%	0.00%	0.22%	0.31%
T-SEA	61.90%	38.10%	50.65%	39.39%	23.59%	21.65%	32.25%	51.52%	36.74%
AdvReal (Ours)	89.39%	77.92%	74.46%	67.32%	67.53%	70.13%	51.08%	59.09%	66.79%

Table 3: ASRs(%) under different IoU thresholds for YOLOv2 and Faster-RCNN detectors

Method	YOLOv2 \uparrow					Faster RCNN \uparrow				
	IoU=0.1	IoU=0.3	IoU=0.5	IoU=0.7	IoU=0.9	IoU=0.1	IoU=0.3	IoU=0.5	IoU=0.7	IoU=0.9
White	0.43%	0.43%	0.65%	6.49%	70.78%	0.22%	0.22%	0.22%	2.16%	53.90%
Gray	0.00%	0.00%	0.00%	7.79%	80.74%	0.00%	0.00%	0.22%	1.30%	68.18%
Random Noise	0.22%	0.00%	0.22%	8.87%	78.79%	0.22%	0.43%	0.43%	2.38%	62.77%
AdvPatch	12.77%	12.99%	14.07%	39.83%	88.96%	0.87%	1.08%	6.06%	22.94%	91.77%
AdvTshirt	11.26%	11.26%	11.26%	29.65%	91.13%	0.43%	0.43%	1.52%	8.87%	87.45%
NatPatch	1.52%	1.52%	1.52%	10.61%	83.33%	0.22%	0.22%	0.22%	1.95%	80.74%
AdvTexture	25.11%	25.54%	25.76%	60.61%	96.97%	2.38%	3.68%	13.64%	41.56%	98.05%
AdvCaT	0.00%	0.00%	0.00%	3.25%	74.46%	0.00%	0.00%	0.00%	0.22%	52.38%
T-SEA	29.00%	30.74%	38.10%	78.14%	98.27%	0.22%	0.43%	67.10%	89.18%	100.00%
AdvReal (Ours)	45.02%	59.31%	86.80%	98.27%	100.00%	6.71%	43.94%	99.57%	99.78%	100.00%

real garments are kept consistent across digital and physical experiments. With the exception of AdvCat, which is entirely camouflaged, the remaining patches and their corresponding garments are shown in Fig. 5.

To comprehensively assess attack performance across continuous video frames and multiple angles, all adversarial patches are printed on long-sleeve tops and trousers. Specifically, six patches are applied to the top—two on the front and back centers and four on the sleeves (one on the front and one on the back of each sleeve)—while eight patches are applied to the trousers, distributed evenly across both legs.

4.2. Digital Adversarial Attack Experiment

4.2.1. Comparisons to SOTA Methods

In Tab. 2, we compare the proposed *AdvReal* with three non-adversarial textures and seven state-of-the-art adversarial patches. YOLOv2 is employed as the glass-box detector, while seven additional closed-box detectors are used to evaluate the adversarial patches.

In the glass-box comparison, influenced by realistic digital world samples, the ASR of previous adversarial patches dropped significantly relative to the results reported in their original papers. Moreover, the ASR of the natural-looking methods—NatPatch (6.06%) and AdvCat (0.00%)—is only marginally higher than that of the three non-adversarial textures. We attribute this lower performance to training approaches that do not sufficiently account for realistic human

body dimensions and authentic lighting conditions. Under closed-box comparison, AdvReal demonstrates superior performance compared to other adversarial methods, including state-of-the-art approaches such as AdvTexture and T-SEA. Notably, when evaluated against the advanced detector YOLOv12, AdvReal achieves an ASR of 70.13%, far exceeding that of T-SEA (21.65%). However, our method’s performance on Faster R-CNN and D-DETR declines, likely due to architectural differences between these detectors and the one used for adversarial training.

To further validate AdvReal’s adversarial performance, we evaluated the ASR of various adversarial patches under different IoU thresholds. As shown in Tab. 3, AdvReal achieves higher ASRs than other attack methods when using both YOLOv2 and Faster R-CNN as detectors. Under the YOLOv2 detector, AdvReal attains an ASR of 45% at an IoU threshold of 0.1—surpassing T-SEA’s 29.00% ASR at an IoU threshold of 0.5. With the Faster R-CNN detector, AdvReal’s ASR approaches 100% at an IoU threshold of 0.5, significantly exceeding T-SEA’s 67.10%. These results indicate that our algorithm performs effectively even under low thresholds and can successfully attack nearly all samples when the threshold is high.

4.3. Ablation Study

Tab. 4 presents ablation experiments that systematically examine the contributions of three modules in the AdvReal framework—namely, non-grid surfaces, Realistic Matching, and

Table 4: Ablation experiment results

Non-grid surfaces	Realistic Matching	Shakedrop Regularization	ASR \uparrow	AC \uparrow
			87.45%	59.68%
✓			91.56%	55.64%
	✓		90.48%	55.39%
		✓	89.18%	58.79%
✓		✓	87.01%	54.28%
	✓	✓	92.42%	55.33%
✓		✓	88.31%	54.84%
✓	✓	✓	93.72%	53.17%

Shakedrop. The results reveal that each module significantly influences both the ASR and the perceptual quality AC of adversarial patches. Specifically, the exclusive use of the non-grid surfaces module boosts ASR from 87.45% to 91.56% while simultaneously lowering AC from 59.68% to 55.64%, thereby enhancing both attack efficacy and visual quality. Similarly, when applied individually, both the Realistic Matching and Shakedrop modules improve ASR and reduce AC. Notably, the Realistic Matching module yields a particularly notable improvement, raising ASR to 90.48% and reducing AC to 55.39%. Interestingly, the combined application of non-grid surfaces and Shakedrop results in a slight ASR decrease to 87.01%, yet it substantially elevates perceptual quality, as evidenced by an AC improvement to 54.28%, indicating a synergistic benefit. Ultimately, the full integration of all three modules delivers optimal performance, achieving an ASR of 93.72% and an AC of 53.17%. These findings ultimately confirm the cumulative effectiveness of the proposed modules, underscoring their synergistic value in balancing attack potency with perceptual quality.

4.4. Robustness

Table 5: Robustness performance of different methods on YOLOv2

Method	YOLOv2			
	ASR \uparrow	Precision \downarrow	Recall \downarrow	F1-Score \downarrow
AdvPatch	26.84%	73.16%	60.68%	60.68%
AdvTshirt	20.56%	56.03%	79.44%	65.71%
NatPatch	3.46%	62.12%	96.54%	75.59%
AdvTexture	21.86%	57.76%	78.14%	66.42%
T-SEA	<u>36.15%</u>	<u>49.50%</u>	<u>63.85%</u>	<u>55.77%</u>
AdvReal	84.20%	14.87%	15.80%	15.32%

When the adversarial patch is partially occluded, its attack efficacy is markedly reduced. To evaluate the robustness of different algorithms under occlusion, we superimpose a 100×100 pixel gray patch at the center of a 300×300 pixel adversarial patch. Tab. 5 compares the robustness performance of various methods under the YOLOv2 glass-box setting. As shown, our method achieves an ASR of 84.20%, far surpassing the second-best method, T-SEA, which records 36.15%. Moreover, AdvReal attains the highest Precision, Recall, and F1-Score (14.87%, 15.80%, and 15.32%, respectively), demonstrating its superior ability to degrade detection performance even under

occlusion. In contrast, other methods—such as AdvPatch, AdvTshirt, and AdvTexture—register ASRs below 30.00% and exhibit considerably lower Precision, Recall, and F1-Scores. Notably, NatPatch achieves an ASR of only 3.46%, likely because it prioritizes natural appearance over adversarial potency. Overall, these results confirm the superior robustness and practical applicability of AdvReal as an adversarial patch.

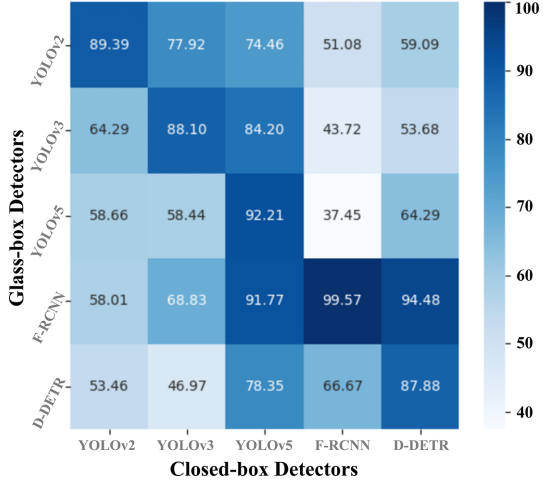


Figure 6: ASRs with different method and IOU thresholds in digital world. The glass-box is Faster RCNN and the confidence threshold is set as 0.5.

4.5. Transferability

4.5.1. Transfer confusion matrix

As illustrated in Fig. 6, we optimized adversarial patches on various detectors to verify the transferability of AdvReal and evaluated their ASRs under both glass-box and closed-box settings. In glass-box tests, AdvReal consistently achieved the highest ASRs—exceeding 90% for YOLOv5 and Faster R-CNN (92.21% and 99.57%, respectively). Although the patch trained on the single-stage YOLO algorithm experienced a significant ASR drop when transferred to the two-stage F-RCNN, it still maintained an ASR above 35.00%. This transferability confirms that AdvReal remains effective under closed-box conditions.

4.5.2. Transfer performance across confidence threshold

We evaluated the ASRs on various closed-box detectors at different confidence thresholds. As shown in Fig. 7, for the YOLOv2 and YOLOv3 detector, adversarial patches trained under the glass-box setting consistently outperformed those trained under the closed-box setting. At a confidence level of 0.7, both glass-box and closed-box patches achieved nearly 100% ASR for YOLOv2. For the YOLOv5 detector, both glass-box and closed-box ASRs exceeded 60% even at a low confidence threshold of 0.1. In the Faster R-CNN detector, the glass-box ASR remained around 100% across confidence thresholds from 0.1 to 0.9. However, due to structural differences relative to the single-stage YOLO and transformer-based D-DETR architectures, the closed-box ASRs remained relatively low until a confidence level of 0.7 was reached. In contrast, for the Deformable-DETR detector, the glass-box ASR was lower than

Table 6: Transferability of different attack methods in YOLOv8, YOLOv11, and YOLOv12

Method	YOLOv8			YOLOv11			YOLOv12		
	Precision ↓	Recall ↓	F1-score ↓	Precision ↓	Recall ↓	F1-score ↓	Precision ↓	Recall ↓	F1-score ↓
AdvPatch	93.64%	57.36%	71.14%	96.50%	77.49%	85.95%	98.72%	83.55%	90.50%
AdvTshirt	96.76%	64.72%	77.56%	97.65%	72.08%	82.94%	98.98%	84.20%	90.99%
NatPatch	97.41%	89.61%	93.35%	97.91%	91.13%	94.39%	99.11%	95.89%	97.47%
AdvTexture	96.50%	71.65%	82.24%	97.03%	77.71%	86.30%	98.93%	80.30%	88.65%
AdvCaT	98.08%	99.35%	98.71%	98.50%	99.57%	99.03%	98.92%	99.13%	99.03%
T-SEA-v2	83.58%	60.61%	70.26%	94.89%	76.41%	84.65%	98.10%	78.35%	87.12%
AdvReal (Ours)	56.55%	32.68%	70.26%	66.37%	32.47%	43.60%	82.63%	29.87%	43.88%

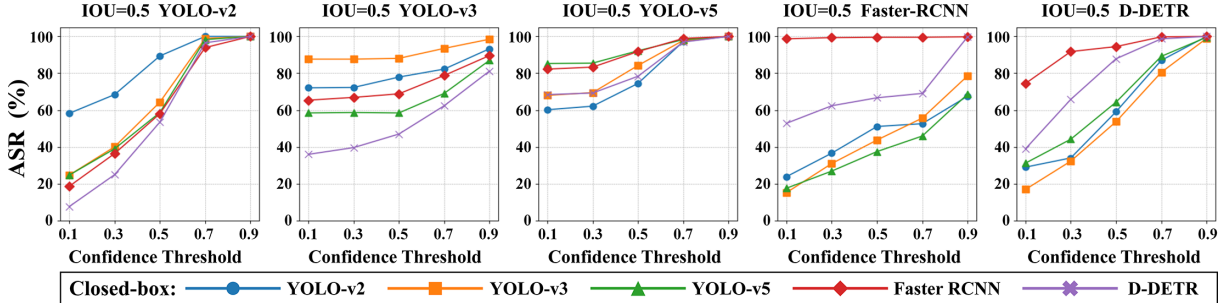


Figure 7: ASRs with different detectors and confidence thresholds in digital world.

the closed-box ASR observed for Faster R-CNN, which can be attributed to the transformer-based architecture of Deformable-DETR that provides greater robustness than other closed-box detectors.

4.5.3. Mobility on advanced detectors

To further verify the transferability of AdvReal to the latest detectors, we evaluated various adversarial attack methods on three state-of-the-art (SOTA) detectors: YOLOv8 (2023s), YOLOv11 (2024s), and YOLOv12 (2025s). As shown in Tab. 6, the results indicate that AdvReal consistently produces significantly lower Precision, Recall, and F1-Scores across all detectors, underscoring its superior effectiveness in degrading object detection performance. Specifically, on YOLOv8, AdvReal achieved Precision, Recall, and F1-Score values of 56.55%, 32.68%, and 70.26%, respectively, outperforming all other methods. Similarly, on YOLOv11 and YOLOv12, AdvReal demonstrated outstanding performance, attaining Precision values of 66.37% and 82.63%, Recall values of 32.47% and 29.87%, and F1-Scores of 43.60% and 43.88%, respectively. In contrast, methods such as AdvPatch, AdvTshirt, and AdvTexture performed substantially worse, particularly in Recall and F1-Score metrics. Notably, although AdvCaT performed reasonably well in Precision and F1-Score, its Recall value was excessively high (nearly 99%), indicating a weaker disruptive capability against the detection models. Overall, AdvReal demonstrated superior transferability across different detectors, confirming its robustness and generalization for cross-model adversarial attacks.

4.6. Physical Adversarial Attack Experiment

The physical adversarial attack experiments were conducted in real-world settings, where human subjects wore adversarial

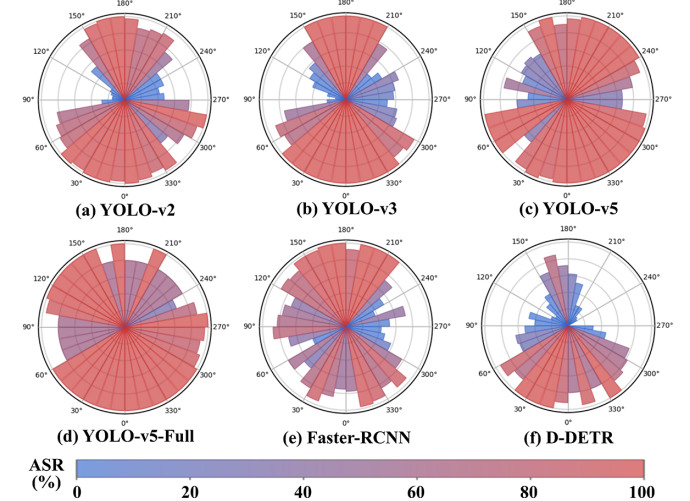


Figure 8: ASRs of adversarial patches trained with different glass-box detectors at various angles.

shirts and pants with printed patches.

4.6.1. All-angle attack

To evaluate the robustness of adversarial patches in real-world applications, we recorded videos of subjects wearing AdvReal-patched clothing while performing a full 360° rotation. For each patch, ten videos with different backgrounds were recorded. We assessed performance consistency across different viewpoints by computing the average ASR at 10 intervals. As shown in Fig. 8, adversarial patches trained on different detectors exhibit distinct angle-dependent attack effectiveness. The experimental results demonstrate that patches achieve better multi-angle attack performance against the single-stage YOLO glass-box detector. In general, all patches exhibit higher

Table 7: Physical-world ASRs of various methods at different distances under adequate lighting conditions

Method	2M ↑	3M ↑	4M ↑
AdvPatch	81.08%	35.14%	27.03%
AdvTshirt	81.08%	72.97%	8.11%
NatPatch	64.86%	13.51%	0.00%
AdvTexture	<u>97.37%</u>	81.58%	21.05%
T-SEA	83.78%	93.75%	81.08%
AdvReal-YOLOv2	81.08%	92.86%	97.30%
AdvReal-YOLOv3	86.49%	<u>97.30%</u>	<u>94.59%</u>
AdvReal-YOLOv5	83.78%	94.59%	97.30%
AdvReal-FRCNN	100.00%	100.00%	91.89%
AdvReal-DDETR	86.49%	91.89%	86.49%

ASRs when facing the camera from the front or back. As the body rotates sideways, the ASR tends to decrease. This drop in performance is attributed to reduced visible patch area and the increased prominence of non-patched human features such as the face, hands, and feet.

4.6.2. Different distances attacks

Tab. 7 and Tab. 8 evaluate the attack performance of clothing printed with different patches under different lighting conditions (adequate light and poor light) and different distances (2m, 3m, 4m). Each patch was taken 111 times at different distances, and the victim model was YOLOv5. In experiments with different distances, the ASR of traditional methods (such as AdvPatch and NatPatch) showed a significant downward trend with increasing distance. However, AdvReal remained stable or even increased. This shows that the distance has little effect on the attack effect. In the case of poor lighting, the method in this paper will have an increase in the attack success rate with increasing distance. This shows that our patch does not depend on certain specific pixels and has very low resolution requirements. It has an attack effect on a macro scale. In the lighting experiment, the ASR of traditional methods dropped sharply in poor light conditions compared to adequate light. However, the attack effects of TSEA, AdvTexture and our method remained stable. This shows that lighting can cause the failure of target

Table 8: Physical-world ASRs of various methods at different distances under poor lighting conditions

Method	2M ↑	3M ↑	4M ↑
AdvPatch	35.14%	12.50%	11.11%
AdvTshirt	100.00%	27.78%	13.89%
NatPatch	2.70%	0.00%	0.00%
AdvTexture	<u>96.67%</u>	<u>83.33%</u>	23.33%
T-SEA	90.00%	94.87%	<u>97.78%</u>
AdvReal-YOLOv2	94.12%	94.44%	34.21%
AdvReal-YOLOv3	52.63%	76.32%	91.89%
AdvReal-YOLOv5	100.00%	100.00%	90.91%
AdvReal-FRCNN	94.59%	100.00%	100.00%
AdvReal-DDETR	53.33%	86.67%	93.33%

detectors and patches. However, the experimental results of the traditional method show that the failure of the patch is dominant. Therefore, the experimental results show that our patch has excellent physical robustness. For the adversarial patches of this paper trained with different target detectors. DDETR is used as a target detector of the transfromer architecture. The attack effect is worse than other target detectors based on convolutional neural networks. It is more robust under attack.

The experimental results show that even under the combined interference of dynamic changes in detection distance and sudden changes in light intensity. The adversarial clothing generation method proposed in this paper still has strong robustness and excellent attack performance.

4.6.3. Visualization and Interpretability

We employed Grad-CAM Selvaraju et al. (2017) to generate activation maps that highlight the regions and salient features the detector attends to during its decision-making process. This helps reveal how AdvReal effectively deceives the object detection system by interfering with its attention. Fig. 9(a) and (b) present visualizations under good and poor lighting conditions in the digital space. In the non-adversarial pedestrian image on the left, the detector’s activation over the target region is smooth and inconspicuous. However, after introducing the adversarial patch, the detector’s attention clearly shifts toward

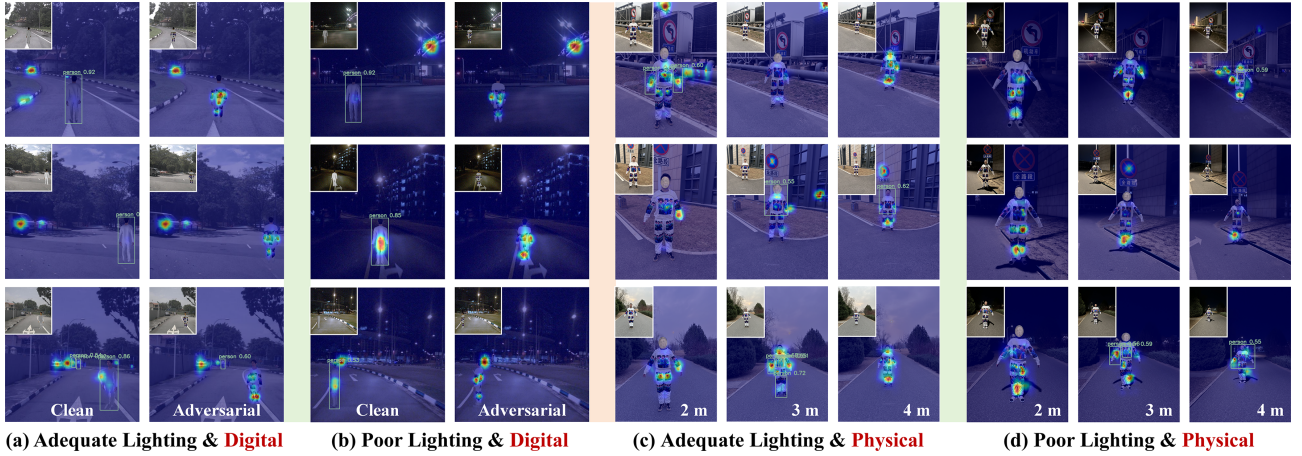


Figure 9: Visual evaluation using Grad-CAM in the digital and physical worlds. (a) and (b) are visualization results under different lighting conditions in the digital world. (c) and (d) are visualization results at different distances in the physical world.

the patch area. A similar trend is observed under poor lighting conditions: the pedestrian receives slightly partial attention, the adversarial patch in the corresponding image still dominates the activation map. In the physical world (Fig. 9(c) and (d)), the detection results and attention distributions at different distances further illustrate that the detector’s focus shifts from the entire pedestrian to the adversarial patch.



Figure 10: Visualization of the proposed adversarial patch and other adversarial patches in the physical world. (a) Glass-box is YOLOv2, closed-box is YOLOv5, and the confidence and IOU thresholds are set to 0.1. (b) Glass-box is YOLOv2, closed-box is YOLOv12, and the confidence and IOU thresholds are set to 0.5.

Fig. 10(a) shows a visualization of the detection box under conditions where $\text{IoU} = 0.1$ and the confidence score is 0.1. In this case, the detector identifies the patch itself as a person with low confidence, which aligns with the observed shift in attention toward the patch. This observation indicates a fundamental change in the detector’s decision-making basis caused by the patch. As shown in Fig. 10(b), when confronting the state-of-the-art detector YOLOv12, AdvReal still successfully misleads the model or significantly suppresses its confidence more effectively than existing adversarial methods, further validating its robustness and transferability.

5. Discussion

5.1. Advantage of Proposed Adversarial Algorithm

5.1.1. Comparative of proposed and other algorithms

Existing physical adversarial methods often overlook the significant discrepancies between digital simulations and real-world scenarios, as well as the inherent diversity and uncertainty present in real environments. As a result, their performance tends to be unstable in practical applications. To address

the limitations, we proposed *AdvReal*, which offers the following key advantages: 1) **Joint 2D-3D Optimization**: *AdvReal* introduces the first joint optimization framework that integrates both 2D and 3D spaces, along with the Shakedrop mechanism, substantially enhancing the transferability of adversarial patches from digital to physical environments. 2) **Realism-Aware Modeling**: The framework explicitly accounts for realistic conditions, such as illumination changes and human body scale variations, ensuring robust and stable attack performance during real-world testing. 3) **Multi-View Robustness**: In contrast to methods trained solely on 2D datasets, *AdvReal* supports multi-view adversarial optimization, enabling it to maintain strong attack effectiveness across a wide range of viewing angles and geometric distortions.

5.1.2. Why 2D-3D joint optimization is effective?

single 2D adversarial optimization often relies on static, idealized patches, while real-world scenarios involve depth, occlusion, perspective distortion, and motion—elements better captured by 3D modeling. Optimizing in both 2D&3D spaces ensures that adversarial patterns remain effective when projected onto real-world surfaces (e.g., curved clothing, variable human angle).

In physical settings, lighting, scaling, and non-rigid modeling play a huge role. 3D rendering allows simulation of these transformations during training, making the patch more robust. Specifically, Tab. 5 shows that *AdvReal* maintains strong adversarial effectiveness even when large portions of the adversarial patches are occluded. Additionally, Tab. 7 and Tab. 8 confirm that *AdvReal* consistently achieves strong adversarial performance even under challenging illumination conditions. Real-world detectors see targets from all angles, and joint optimization helps enforce effectiveness from multiple viewpoints. Fig. 8 further illustrates performance across various viewing angles, highlighting that *AdvReal* achieves excellent attack results on YOLO detectors, despite slightly reduced effectiveness on robust detectors such as Faster R-CNN and D-DETR. In summary, 3D optimization can effectively supplement the shortcomings of traditional adversarial optimization methods in the physical world.

5.1.3. Discoveries and recommendations of AI-safety in object detection system for AVs

The results reveals that the vulnerability of object detectors to physical adversarial patches varies considerably across different architectures. Single-stage detectors such as YOLOv11 and YOLOv12 are more to adversarial manipulation, while the earlier YOLOv8 version demonstrates higher robustness (Tab. 2 and Fig. 6). Two-stage detectors like Faster R-CNN exhibit greater resistance to physical attacks, likely due to its huge model parameters and intermediate region proposal mechanism that helps filter out adversarial cues Ren et al. (2016b). Meanwhile, transformer-based models such as D-DETR show even stronger robustness under multi-view conditions, maintaining stable performance across varying viewpoints (Fig. 8).

In the context of autonomous driving, image perception systems must strike a balance between real-time processing and

resilience to adversarial threats. The experiments indicate that adversarial patches can significantly redirect the detector’s attention away from semantically meaningful regions, resulting in missed detections (Fig. 9 and Fig. 10). To mitigate these risks, we recommend reinforcing the structural robustness of detection models. Multi-stage and transformer-based architectures exhibit stronger spatial awareness and adversarial resistance. Moreover, detection heads should be equipped with mechanisms such as attention stabilization or feature denoising modules to counteract patch-induced interference. In summary, the development of safety-aware detectors requires not only stronger model architectures but also defense strategies grounded in real-world adversarial behavior.

5.2. Limitations of Proposed Adversarial Algorithm

Although AdvReal demonstrates superior adversarial performance compared to other methods in both digital and physical experiments, it still has certain potential limitations.

(a) Limitations of the attack mechanism. The attack success rate 0 of the adversarial patch generated by the glass-box attack in a closed-box detector is significantly reduced, especially when targeting two-stage and transformer-based detectors. In these cases, the attack success rate of the single-stage adversarial patch drops to a minimum of 37.45% (Fig. 6). This is a common problem faced by current adversarial attacks. The difference in feature space between the unified feature map prediction of the single-stage detector and the step-by-step feature processing in the two-stage detector prevents effective alignment of the adversarial perturbation information. *Shakedrop* and other strategy have slightly improved the transferability by changing the complexity of the model. However, a generalized training framework is still required to address the limitation of over-reliance on adversarial attacks.

(b) Fight against the shape constraints of the patch. The proposed AdvReal method mainly focuses on adversarial effectiveness and does not effectively constrain the nature looking of generated patches. Consequently, adversarial patches may appear visually unnatural and easily detectable, limiting their use in scenarios requiring visual subtlety. Future research could further explore achieving a better balance between adversarial effectiveness and nature looking.

6. Conclusion and Future works

This study proposed AdvReal, a robust adversarial patch generation framework designed to address challenges in physical-world attacks on object detection systems, including intra-class diversity, multi-angle variations, and complex environmental conditions. By incorporating 2D–3D joint optimization, physics-driven non-rigid surface modeling, and a realistic matching mechanism for lighting and geometry, AdvReal effectively bridges the gap between digital simulations and physical scenarios, thereby enhancing the transferability and robustness of adversarial patches. Experimental results across diverse

object detectors and real-world settings demonstrate that AdvReal achieves state-of-the-art attack success rates, superior resilience to occlusion and lighting variations, and notable efficacy in redirecting detector attention. The proposed framework underscores the critical role of realistic 3D modeling and joint training in overcoming the limitations of conventional methods, providing a foundational benchmark for evaluating the adversarial robustness of AVs perception systems.

Looking ahead, several promising research directions warrant exploration to further enhance the framework and address current limitations. First, improving the generalization capability of adversarial patches across heterogeneous detector architectures requires consideration of structural differences in feature extraction and decision-making processes. Second, balancing adversarial effectiveness with visual naturalness could lead to more covert and practical attacks. Lastly, insights derived from AdvReal may inform the design of robust defense mechanisms, such as attention-stabilized detection modules or adversarial patch-aware training, to strengthen the resilience of intelligent object detection systems.

References

- Abed, A., Akroud, B., Amous, I., 2024. Deep learning-based few-shot person re-identification from top-view rgb and depth images. *Neural Computing and Applications* 36, 19365–19382.
- Agudo, A., Moreno-Noguer, F., 2017. Force-based representation for non-rigid shape and elastic model estimation. *IEEE transactions on pattern analysis and machine intelligence* 40, 2137–2150.
- Bai, X., Dong, P., Huang, Y., Kumari, S., Yu, H., Ren, Y., 2024. An ar-based meta vehicle road cooperation testing systems: framework, components modeling and an implementation example. *IEEE Internet of Things Journal* .
- Brown, T.B., Mané, D., Roy, A., Abadi, M., Gilmer, J., 2017. Adversarial patch. *arXiv preprint arXiv:1712.09665* .
- Caesar, H., Bankiti, V., Lang, A.H., Vora, S., Lioung, V.E., Xu, Q., Krishnan, A., Pan, Y., Baldan, G., Beijbom, O., 2020. nuscenes: A multimodal dataset for autonomous driving, in: *Proceedings of the IEEE/CVF conference on computer vision and pattern recognition*, pp. 11621–11631.
- Carion, N., Massa, F., Synnaeve, G., Usunier, N., Kirillov, A., Zagoruyko, S., 2020. End-to-end object detection with transformers, in: *European conference on computer vision*, Springer. pp. 213–229.
- Chow, K.H., Liu, L., Loper, M., Bae, J., Gursoy, M.E., Truex, S., Wei, W., Wu, Y., 2020. Adversarial objectness gradient attacks in real-time object detection systems, in: *2020 Second IEEE International Conference on Trust, Privacy and Security in Intelligent Systems and Applications (TPS-ISA)*, IEEE. pp. 263–272.
- Cui, J., Guo, W., Huang, H., Lv, X., Cao, H., Li, H., 2024. Adversarial examples for vehicle detection with projection transformation. *IEEE Transactions on Geoscience and Remote Sensing* .
- Dalal, N., Triggs, B., 2005. Histograms of oriented gradients for human detection, in: *2005 IEEE computer society conference on computer vision and pattern recognition (CVPR’05)*, Ieee. pp. 886–893.
- Fang, J., Jiang, Y., Jiang, C., Jiang, Z.L., Liu, C., Yiu, S.M., 2024. State-of-the-art optical-based physical adversarial attacks for deep learning computer vision systems. *Expert Systems with Applications* , 123761.
- Giri, K.J., et al., 2025. So-yolov8: A novel deep learning-based approach for small object detection with yolo beyond coco. *Expert Systems with Applications* , 127447.
- Guesmi, A., Ding, R., Hanif, M.A., Alouani, I., Shafique, M., 2024. Dap: A dynamic adversarial patch for evading person detectors, in: *Proceedings of the IEEE/CVF Conference on Computer Vision and Pattern Recognition*, pp. 24595–24604.
- Gundogdu, E., Constantin, V., Parashar, S., Seifoddini, A., Dang, M., Salzmann, M., Fua, P., 2020. Garnet++: Improving fast and accurate static 3d cloth draping by curvature loss. *IEEE Transactions on Pattern Analysis and Machine Intelligence* 44, 181–195.

Hingun, N., Sitawarin, C., Li, J., Wagner, D., 2023. Reap: a large-scale realistic adversarial patch benchmark, in: Proceedings of the IEEE/CVF International Conference on Computer Vision, pp. 4640–4651.

Hu, Y.C.T., Kung, B.H., Tan, D.S., Chen, J.C., Hua, K.L., Cheng, W.H., 2021. Naturalistic physical adversarial patch for object detectors, in: Proceedings of the IEEE/CVF International Conference on Computer Vision, pp. 7848–7857.

Hu, Z., Chu, W., Zhu, X., Zhang, H., Zhang, B., Hu, X., 2023. Physically realizable natural-looking clothing textures evade person detectors via 3d modeling, in: Proceedings of the IEEE/CVF Conference on Computer Vision and Pattern Recognition, pp. 16975–16984.

Hu, Z., Huang, S., Zhu, X., Sun, F., Zhang, B., Hu, X., 2022. Adversarial texture for fooling person detectors in the physical world, in: Proceedings of the IEEE/CVF conference on computer vision and pattern recognition, pp. 13307–13316.

Huang, G., Sun, Y., Liu, Z., Sedra, D., Weinberger, K.Q., 2016. Deep networks with stochastic depth, in: Computer Vision–ECCV 2016: 14th European Conference, Amsterdam, The Netherlands, October 11–14, 2016, Proceedings, Part IV 14, Springer. pp. 646–661.

Huang, H., Chen, Z., Chen, H., Wang, Y., Zhang, K., 2023. T-sea: Transfer-based self-ensemble attack on object detection, in: Proceedings of the IEEE/CVF conference on computer vision and pattern recognition, pp. 20514–20523.

Huang, Y., Zhang, Q., Xing, J., Cheng, M., Yu, H., Ren, Y., Xiong, X., 2024. Advswap: Covert adversarial perturbation with high frequency info-swapping for autonomous driving perception, in: 2024 IEEE 27th International Conference on Intelligent Transportation Systems (ITSC), pp. 1686–1693. doi:10.1109/ITSC58415.2024.10920187.

Jing, L., Wang, R., Ren, W., Dong, X., Zou, C., 2024. Pad: Patch-agnostic defense against adversarial patch attacks, in: Proceedings of the IEEE/CVF Conference on Computer Vision and Pattern Recognition, pp. 24472–24481.

Jocher, G., Chaurasia, A., Qiu, J., 2023. Ultralytics yolov8. URL: <https://github.com/ultralytics/ultralytics>.

Jocher, G., Qiu, J., 2024. Ultralytics yolo11. URL: <https://github.com/ultralytics/ultralytics>.

Jocher, G., Stoken, A., Borovec, J., Changyu, L., Hogan, A., Diaconu, L., Poznanski, J., Yu, L., Rai, P., Ferriday, R., et al., 2020. ultralytics/yolov5: v3. 0. Zenodo .

Li, Y., Zhang, W., Liang, K., Xiao, B., 2025. Uv-attack: Physical-world adversarial attacks for person detection via dynamic-nerf-based uv mapping. arXiv preprint arXiv:2501.05783 .

Lin, T.Y., Maire, M., Belongie, S., Hays, J., Perona, P., Ramanan, D., Dollár, P., Zitnick, C.L., 2014. Microsoft coco: Common objects in context, in: Computer vision–ECCV 2014: 13th European conference, zurich, Switzerland, September 6–12, 2014, proceedings, part v 13, Springer. pp. 740–755.

Liu, X., Shen, F., Zhao, J., Nie, C., 2024. Eap: An effective black-box impersonation adversarial patch attack method on face recognition in the physical world. Neurocomputing 580, 127517.

Maesumi, A., Zhu, M., Wang, Y., Chen, T., Wang, Z., Bajaj, C., 2021. Learning transferable 3d adversarial cloaks for deep trained detectors. arXiv preprint arXiv:2104.11101 .

Mahima, K.Y., Perera, A.G., Anavatti, S., Garratt, M., 2024. Toward robust 3d perception for autonomous vehicles: A review of adversarial attacks and countermeasures. IEEE Transactions on Intelligent Transportation Systems .

Ran, Y., Zhang, A.X., Li, M., Tang, W., Wang, Y.G., 2025. Black-box adversarial attacks against image quality assessment models. Expert Systems with Applications 260, 125415.

Redmon, J., 2018. Yolov3: An incremental improvement. arXiv preprint arXiv:1804.02767 .

Redmon, J., Farhadi, A., 2017. Yolo9000: better, faster, stronger, in: Proceedings of the IEEE conference on computer vision and pattern recognition, pp. 7263–7271.

Redmon, J., Farhadi, A., 2018. Yolov3: An incremental improvement. URL: <https://arxiv.org/abs/1804.02767>, arXiv:1804.02767.

Ren, S., He, K., Girshick, R., Sun, J., 2016a. Faster r-cnn: Towards real-time object detection with region proposal networks. IEEE transactions on pattern analysis and machine intelligence 39, 1137–1149.

Ren, S., He, K., Girshick, R., Sun, J., 2016b. Faster r-cnn: Towards real-time object detection with region proposal networks. URL: <https://arxiv.org/abs/1506.01497>, arXiv:1506.01497.

Selvaraju, R.R., Cogswell, M., Das, A., Vedantam, R., Parikh, D., Batra, D., 2017. Grad-cam: Visual explanations from deep networks via gradient-based localization, in: Proceedings of the IEEE international conference on computer vision, pp. 618–626.

Swerdlow, A., Xu, R., Zhou, B., 2024. Street-view image generation from a bird’s-eye view layout. IEEE Robotics and Automation Letters .

Thys, S., Van Ranst, W., Goedemé, T., 2019. Fooling automated surveillance cameras: adversarial patches to attack person detection, in: Proceedings of the IEEE/CVF conference on computer vision and pattern recognition workshops, pp. 0–0.

Tian, Y., Ye, Q., Doermann, D., 2025. Yolov12: Attention-centric real-time object detectors. arXiv preprint arXiv:2502.12524 .

Wang, D., Jiang, T., Sun, J., Zhou, W., Gong, Z., Zhang, X., Yao, W., Chen, X., 2022. Fca: Learning a 3d full-coverage vehicle camouflage for multi-view physical adversarial attack, in: Proceedings of the AAAI conference on artificial intelligence, pp. 2414–2422.

Wang, L., Huang, J., Huang, L., Wang, F., Gao, C., Li, J., Xiao, F., Luo, D., 2024. Attention-disentangled re-id network for unsupervised domain adaptive person re-identification. Knowledge-Based Systems 304, 112583.

Wei, H., Tang, H., Jia, X., Wang, Z., Yu, H., Li, Z., Satoh, S., Van Gool, L., Wang, Z., 2024. Physical adversarial attack meets computer vision: A decade survey. IEEE Transactions on Pattern Analysis and Machine Intelligence .

Wei, X., Guo, Y., Yu, J., Zhang, B., 2022. Simultaneously optimizing perturbations and positions for black-box adversarial patch attacks. IEEE transactions on pattern analysis and machine intelligence 45, 9041–9054.

Williams, P., Li, K., 2024. Camopatch: An evolutionary strategy for generating camouflaged adversarial patches. Advances in Neural Information Processing Systems 36.

Xiao, C., Peng, S., Zhang, L., Wang, J., Ding, D., Zhang, J., 2025. A transformer-based adversarial network framework for steganography. Expert Systems with Applications 269, 126391.

Xu, K., Zhang, G., Liu, S., Fan, Q., Sun, M., Chen, H., Chen, P.Y., Wang, Y., Lin, X., 2020. Adversarial t-shirt! evading person detectors in a physical world, in: Computer Vision–ECCV 2020: 16th European Conference, Glasgow, UK, August 23–28, 2020, Proceedings, Part V 16, Springer. pp. 665–681.

Yamada, Y., Iwamura, M., Kise, K., 2018. Shakedrop regularization. URL: <https://openreview.net/forum?id=S1NHaMW0b>.

Zhang, J., Lou, Y., Wang, J., Wu, K., Lu, K., Jia, X., 2021. Evaluating adversarial attacks on driving safety in vision-based autonomous vehicles. IEEE Internet of Things Journal 9, 3443–3456.

Zhang, X., Huang, J., Huang, Y., Huang, K., Yang, L., Han, Y., Wang, L., Liu, H., Luo, J., Li, J., 2022. Intelligent amphibious ground-aerial vehicles: State of the art technology for future transportation. IEEE Transactions on Intelligent Vehicles 8, 970–987.

Zhou, D., Qu, H., Wang, N., Peng, C., Ma, Z., Yang, X., Gao, X., 2025. Fooling human detectors via robust and visually natural adversarial patches. Neurocomputing 616, 128915.

Zhou, M., Zhou, W., Huang, J., Yang, J., Du, M., Li, Q., 2024. Stealthy and effective physical adversarial attacks in autonomous driving. IEEE Transactions on Information Forensics and Security .

Zhu, X., Su, W., Lu, L., Li, B., Wang, X., Dai, J., 2020. Deformable detr: Deformable transformers for end-to-end object detection. arXiv preprint arXiv:2010.04159 .